Research Article Vol. 26, No. 18 | 3 Sep 2018 | OPTICS EXPRESS 24114
Optics EXPRESS

Residual-stress-induced helical long period fiber gratings for sensing applications

ZILIANG LI, SHEN LIU,* ZHIYONG BAI, CAILING FU, YAN ZHANG, ZHONGYUAN SUN, XUEYA LIU, AND YIPING WANG

Key Laboratory of Optoelectronic Devices and Systems of Ministry of Education and Guangdong Province, College of Optoelectronic Engineering, Shenzhen University, Shenzhen 518060, China
*liushen.szu@gmail.com

Abstract: We demonstrate a high-efficiency grating fabrication system, which can be used to inscribe a high-quality helical long period fiber grating (HLPFG) on single-mode fiber by means of hydrogen-oxygen flame. Such the HLPFG can be produced in enormous quantities with a uniform grating parameters and good reproducibility of grating inscription. Possible mechanisms for refractive index modulation in the HLPFG can be attributed to residual stress concentration by solidifying the periodic twisting stress under a fused status of optical fiber. Moreover, the HLPFG exhibits an excellence performance of high temperature sensing with a high sensitivity of ~132.8 pm/°C and a measuring range from room temperature to 900 °C. Comparing to the traditional LPFG fabricated by CO_2 laser or arc discharge technique, the HLPFG has a low the bending and tensile strain sensitivity of 1.94 nm/(1/m) and 1.41 pm/με, respectively. So the proposed HLPFG could have a great potential in special applications as optical high-temperature sensors.

1. Introduction

Long period fiber gratings (LPFGs) already play a vital role in a variety of fields, such as optical sensors, communication, wavelength rejection, and filters [1–4]. For fabricating a LPFG on a single mode fiber, a number of fabrication methods has been reported, which including ultraviolet (UV) laser exposure [5,6], CO_2 laser irradiation [7–9], electric-arc discharge [10], femtosecond laser micromachining [11], ion-beam irradiation [12], mechanical micro-bends [13,14], fiber heating-taper periodically [15], and so on. Such the LPFG based on devices have also been written in different types of optical fiber, and developed to realize their sensing and communication application. Generally, the reported mechanisms of forming a LPFG in optical fiber is based on the refractive index modulating periodically, which is attributed to residual stress relaxation, glass densification, or physical deformation [1]. For example, B. H. Kim, et al. [16] reported that the residual stress relaxation is the main mechanism for the LPFG with refractive-index change written by CO_2 laser in optical fiber. Liu et al. [17] reported that the glass structure of optical fiber was changed into the volume increasing or densification while this fiber was heated. Another main fabrication mechanisms is the physical deformation, which was achieved by Wang et al. [13], Sakata et al. [14] and Grellier et al. [18]. Helical long period fiber gratings (HLPFGs) have been proposed and demonstrated in last few years [19–22]. Poole et al. are the first to demonstrate the helical structure of a LPFG fabricated with wiring for a two-mode fiber spatial-mode coupler [23]. Comparing with traditional LPFGs, HLPFGs have a larger measurement range and higher sensitivity on torsional parameters because of different formation mechanism and physical characteristics [22]. Recently, various in-fiber generator of orbital angular momentum (OAM) have been widely researched, especially based on a HLPFG, which has been reported in [24] to generate the OAM ± 1 mode with a stable vortex phase while the temperature increased from 23 to 50 °C. Higher order OAM ± 2 has been demonstrated by twisting a four mode fiber (4MF) by means of CO_2 [25]. In addition, an in-fiber OAM generator based on a HLPFG has been reported in [26] to generate the OAM_{+1}

#338495 https://doi.org/10.1364/OE.26.024114
Journal © 2018 Received 12 Jul 2018; revised 15 Aug 2018; accepted 27 Aug 2018; published 31 Aug 2018

mode with a conversion efficiency of 87% and purity of 91%. However, the sensing characteristics of HLPFG created by hydrogen-oxygen flame heating have never been reported yet.

In this letter, we experimentally demonstrated a HLPFG inscribed in a single mode fiber (SMF, Corning SMF-28). Such the HLPFG is written by twisting the SMF during hydrogen-oxygen flame heating. Possible mechanisms for refractive index modulation in the HLPFG can be attributed to residual stress concentration by solidifying the periodic helical stress under a fused status of optical fiber. Comparing with the conventional LPFGs fabricated by scanning CO_2 laser or electric-arc discharge, the HLPFG has an ultra-smooth and uniform grating surface without any deformation along fiber axis direction. Furthermore, we measure the sensing response of HLPFG for the applied temperature, bending and tensile strain. The experimental results illustrate that the HLPFG can be developed a high-temperature sensor with a sensitivity of ~132.8 pm/°C. Contrasting to the reported LPFG, the HLPFG our proposed has a lower sensitivity to the applied bending and tensile strain.

2. Residual-stress-induced HLPFG

2.1 High-efficiency grating fabrications

In order to inscribe HLPFG on single mode fiber, we have created a fabrication system, which consist of a high-precision rotator, two translational platforms, and a hydrogen-oxygen flame (HOF), and the corresponding assembly drawing of there is illustrated in Fig. 1. During a whole process of fabricating HLPFG, the rotator is fixed on the left translation stage, and this combinatorial set-up can provide a stable rotating angle and linear moving speed. The right translation stage can also contribute to a stable moving speed. The HOF, producing from a hydrogen generator, is utilized to heat an employed optical fiber. All of devices mentioned above, can be controlled by a LabVIEW soft with a friendly operating interface. As shown in Fig. 1, the detailed fabrication process of HLPFG in a SMF is described in [26]. The corresponding helical pitch (Λ) of HLPFG can be calculated by

$$\Lambda = 60\, V_2/\Omega \tag{1}$$

where Ω (rpm) is a rotated rate and V_2(mm/s) is a moving velocity, respectively.

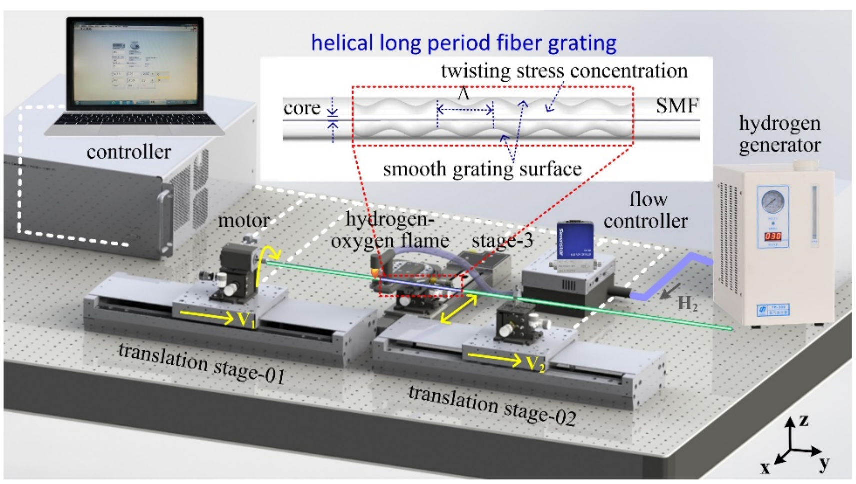

Fig. 1. Schematic diagram of HLPFG inscription by use of a hydrogen-oxygen flame, and the insert is a schematic diagram of a helical long period fiber grating (HLPFG).

For demonstrating the high-efficient, high-quality and repeatability of the HLPFG fabrication system mentioned above, as shown in Fig. 2, three HLPFG samples (HLPFG-1, HLPFG-2, and HLPFG-3) were fabricated with different rotated rate of 183, 189, and 192 rpm (i.e. grating pitches to be524.5, 507.9, and 492.3 μm), respectively. The transmission spectrum of HLPFG samples are measured covering wavelength range from 1250 to 1650 nm, where the optical measurement setup are employed consisting of an amplified spontaneous emission source (ASE, NKT Photonics) and an optical spectral analyzer (OSA, Model AQ6370C) with a resolution of 0.1 nm. The corresponding resonant wavelength of three HLPFG samples is measured to be 1558.6, 1506.32, and 1459.72 nm, corresponding to coupling strength of −34.76, −35.48, and −36.38 dB, respectively. Here, the fabricated speed V_2 is set to be 1.6 mm/s, and the HLPFG grating length of three samples are cut to be about 16.8, 16.2, and 15.7 mm, where the cutting accuracy depends on a computer-controlled precision cleaving system [26,27]. As a result, it only takes about 10 seconds to process a HLPFG grating sample, which indicates that the HLPFG fabrication system is more high-efficient than that of conventional grating inscription method [6,10,28]. In addition, it is noteworthy that, using the HLPFG fabrication system, we can fabricate a twisted fiber with length of 600 mm once, which means that 37 HLPFGs with the same grating length can be fabricated at one time. Furthermore, the HLPFG samples have a high-quality transmission spectrum, and insertion losses are measured to be about 0.2 dB illustrated in Fig. 2. The HLPG fabrication system has a good stability and repeatability. Once pre-setting the values of the rotated rate Ω (rpm) and move velocity V_2 (mm/s), the fabricated HLPFGs under the same grating length will have almost the uniform position of resonant wavelength, which are validated in [26].

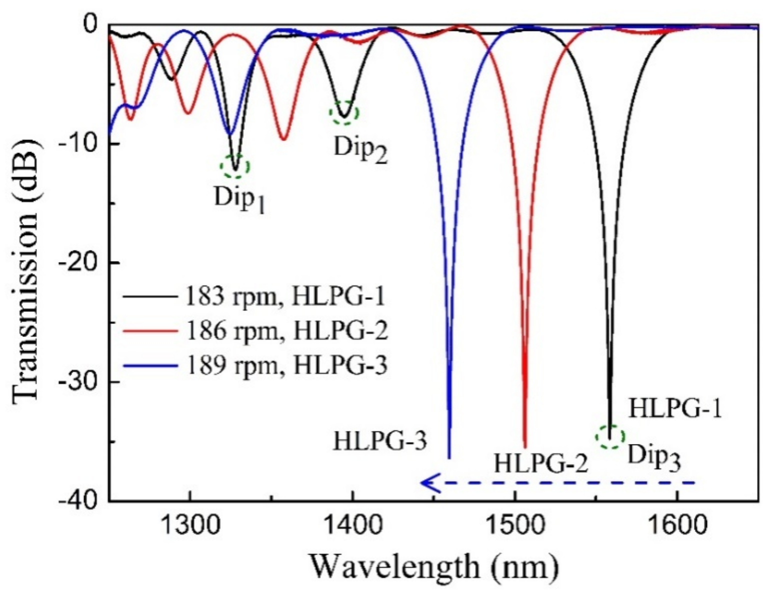

Fig. 2. The transmission spectra of three HLPFG samples (HLPFG-1, HLPFG-2, and HLPFG-3)with different resonant wavelength of 1558.6, 1506.32, and 1459.72 nm, corresponding to different rotated rate of 183, 189 and 192 rpm, respectively.

2.2 Residual-stress reserve

For investigating the possible mechanisms for refractive index modulation in the HLPFG, as shown in Fig. 3(a), one HLPFG sample is fabricated by set a series of motion parameters, such as, V_1 and V_2 are installed the values as 1.38 and 1.60 mm/s with a certain velocity difference, and a rotated rate Ω is a value 186 (rpm). As a result, using Eq. (1), the grating pitch is calculated to 516.13μm corresponding to a resonant wavelength of 1549.8 nm.

In order to determine the actual structure of this HLPFG sample, a scanning electron microscope (SEM) along fiber axis direction and grating cross-section are illustrated in Figs.

3(c) and 3(d), respectively. In the range of 1900 μm, it can be observed that no mechanical deformation on the surface of twisted fiber, except the size of fiber's diameter decreased from 125 to 118 μm, which is due to pre-set a certain velocity difference (V_2-V_1 = 0.22 mm/s). This smooth surface also proves that the residual stress concentration based on a fused-twisting-solidified process is essential reason to form the HLPFG on the SMF, which completely subverts the traditional interpretation of the residual stress relaxation based on CO_2-laser-induced LPFG [1]. Furthermore, the fabrication process of HLPFG can be considered as a fused-solidified heating process, which is that, as soon as the fused fiber with a twisted stress is moved away from the HOF, the periodic helical structures are solidified immediately, and then periodic residual stress is reserved in the helical fiber. Here, the grating pitch depend on the solidified velocity V_2 (i.e. the velocity away from HOF) and the rotated rate Ω (rpm), i.e. the values of V_2 and Ω determine the distribution range of residual stress along the axial and across-section direction of the optical fiber, respectively. As a result, the possible mechanisms for refractive index modulation in the HLPFG can be attributed to residual stress reserve by solidifying the periodic twisting stress under a fused status of optical fiber.

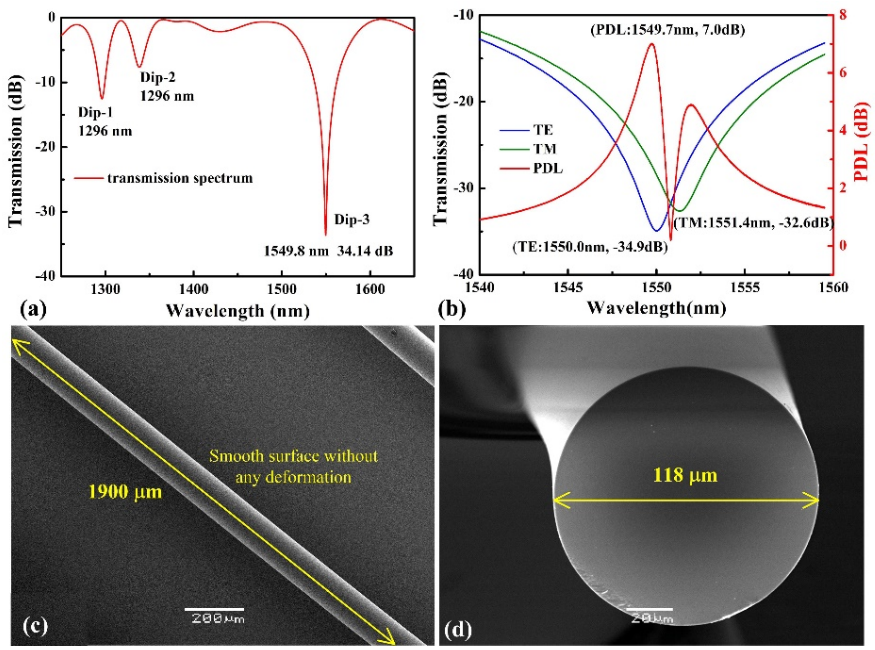

Fig. 3. (a) The transmission spectrum of a high-quality HLPFG's sample with a wavelength range from 1250 to 1650 nm; (b) The measured transmission spectrum(corresponding to the two orthogonal polarizations: TE (blue) and TM (green)polarizations)and the PDL curve (red) of this sample; (c) The SEM along fiber axis direction and (d) SEM across-section of the HLPFG's sample.

As shown in Fig. 3(b), the polarization-dependent loss (PDL) of this sample is measured at the resonant wavelength, by employing the measurement devices of a tunable laser (Agilent Model 81940A), a polarization synthesizer (Agilent Model N7786B), and an optical power meter (Agilent Model N7744A). The result is shown that the HLPFG sample has a maximum PDL is 7.0 dB closed to resonant wavelength, resulting from the asymmetric azimuthal profile of refractive index modulation in the twisted optical fiber. Furthermore, PDL is defined as the maximum change in the transmitted power for polarizations, and it is sensitive to the dip attenuation of the transmission spectrum [22]. This sample has a large dip attenuation of –34.14 dB at the resonant wavelength with a maximum PDL 7.0 dB, which is twice times greater than that of reported in [26] due to its low dip attenuation of –26.7 dB.

Optics EXPRESS

3. HLPFG sensing applications

To illustrate the sensing characteristics of HLPFG based on residual stress concentration, as following discussions, its sensing responses of temperature, tensile strain, and bending, are described in detail.

3.1 high-temperature sensing

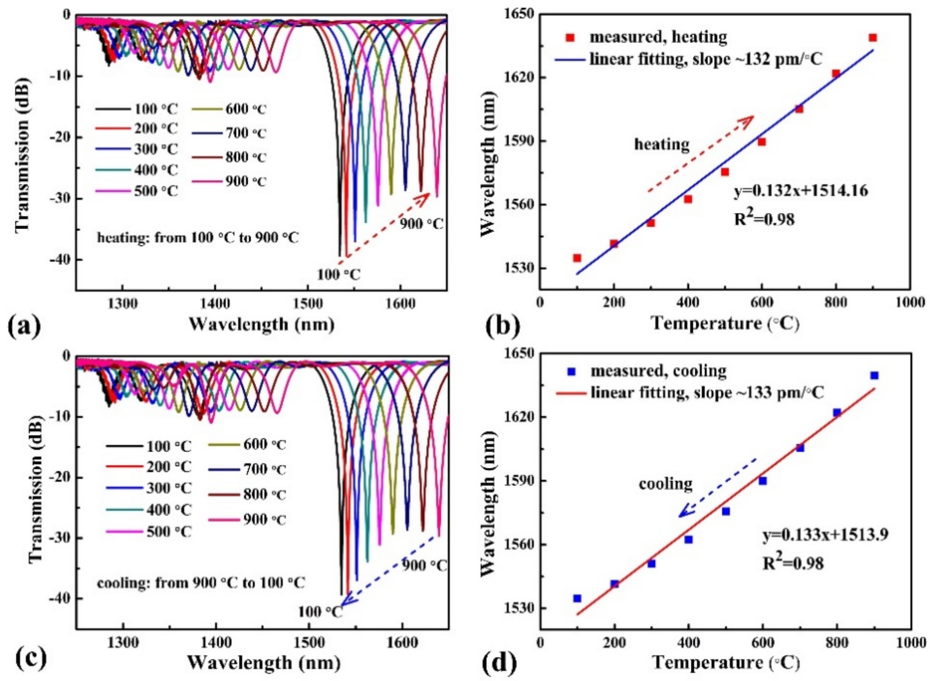

Fig. 4. (a) The spectral evolution of the sample-A with the temperature rising from 100 ℃ to 900 ℃, and (b) the temperature sensitivity is obtained to be about 132 pm/℃. (c) The spectral evolution of the sample-A with the temperature cooling down from 900 ℃ to 100 ℃, and (d) corresponding to a temperature sensitivity of ~133 pm/℃.

In order to measure the temperature response, as shown in Fig. 4, a sample-A of HLPFG with 507.9 μm grating pitch and 36 grating period numbers was fabricated by means of the HLPFG fabrication system mentioned in Fig. 1. The corresponding resonant wavelength is 1528.6 nm at the room temperature. Firstly, the sample-A is placed in an electrical tubular-oven (Cabolite EST 12/300B-230SN), which can reach a temperature as high as 1200°C. The sample-A is loosely placed in the electrical tubular-oven with no external stress applied. The temperature is raised up to 1000 °C, this temperature is maintained 2 hours used for HLPFG's annealing, and then cooled down to room temperature with a slow change of temperature. Next, the applied temperature is raised from a room temperature to 900 °C with a step of 100 °C, and the transmission spectrum evolution of sample-A is shown in Fig. 4(a) with a raising temperature. Here, when a desired temperature is achieved each time, the temperature is maintained for 30 min, and then the resonant wavelength of the sample-A is also recorded. As shown in Fig. 4(a), the corresponding spectral evolution versus applied temperature is presented more clearly, from this results, it can be seen that the resonant wavelength shifts toward a longer wavelength with an increasing temperature. Furthermore, the process of cooling temperature has been illustrated in Fig. 4(c) from 900 °C to 100 °C, and the recorded results show that the resonant wavelength shifts toward short wavelength. The linear fitting to the wavelength changes of sample, as shown in Figs. 4(b) and 4(d), provide a slope of ~132.0 and ~133 pm/ °C, respectively, which is more one order of magnitude greater than that of I-LPFG reported in [29]. In addition, the temperature sensitivity of HLPFG our proposed is about 2.3 times higher than the reported LPFGs in [1], and reported HLPG in [30] by using a CO_2 laser technique with temperature sensitivities of ~58 and ~52 pm/°C, respectively. Note that, in the whole annealing experiment, the change of the HLPFGs' transmission spectrum is almost same as the conventional LPFG annealing, i.e. the resonant wavelength is unstable, which occurs as a sharp wavelength shift at a high temperature. It is necessary to anneal the LPFGs, and appropriate anneal times will depend on the fiber type and the fabrication method of LPFGs, as well as on the required stability of the grating device. For example, Ashish et al. [3] has reported a LPFG induced by UV-laser, which is annealed in order to remove unreacted hydrogen and unstable UV-induced defects, and then stable high temperature sensing characteristics can be obtained. Rao et al. [31] has reported the annealing experiment of LPFG fabricated by CO_2 laser, and the result has indicated that the annealing greatly enhances the linearity and repeatability of the LPFG temperature response.

3.2 strain sensing

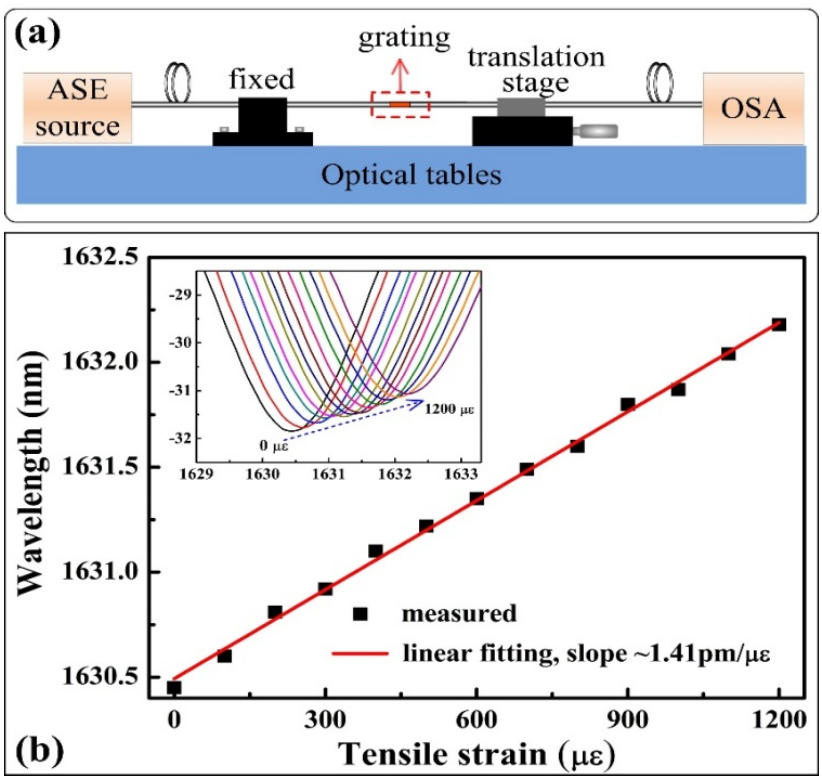

Fig. 5. (a) Schematic diagram of the experimental setup used for applying a continuous strain; (b) Measured resonant wavelength of sample-B as a function of tensile strain. Inset: transmission spectrum evolution of sample-B while the tensile strain increases from 0 to 1200με.

As shown in Fig. 5, we investigate the strain response of a HLPFG sample-B with grating pitch of 524.5 μm and grating length of 16.80 mm, where the sample-B has a resonant wavelength of 1630.4 nm and coupling strength over −31 dB. Figure 5(a) shows the experimental setup used for applying a continuous strain, in which one end of sample-B is fixed and glued onto a holder, which is anchored in the optical tables by binding screw. And then, the other end of sample-B is attached to a translation stage with a step resolution of 10

Optics EXPRESS

μm by a strongly glue. The total length of the stretched fiber, including the single mode fiber and HLPFG, is 200 mm. As shown in Fig. 5(b), the wavelength shift of the transmission fringe around 1630 nm, is measured while the tensile strain is increased from 0 to 1200 με with a step of 100 με, where the OSA is employed with a resolution of 0.02 nm. The inset shows the transmission spectrum evolution of the sample-B with tensile strain increasing. As a result, the strain sensitivity of sample-B is obtained by fitting the dip of wavelength change, and the corresponding slope is about 1.41 pm/με, which is similar than that of the conventional CLPGs [32] with a strain sensitivity of 1.75 pm/με, fabricated by scanning CO_2 laser. Furthermore, an ultra-sensitivity strain sensor has been reported in [33] with sensitivity of 43.0 pm/με. In our experiment, the Corning SMF-28 is utilized to fabricate HLPFGs and the dip wavelength would be shifted to long wavelength direction with increment of the applied strain. The shifted direction of dip wavelength depends on many factors, such as optical fiber type, grating period number and cladding mode order [3,28,34]. Ashish M. et al. [3] has compared the strain response of two LPFGs fabricated by different optical fiber, one show a strain sensitivity of –0.7 pm/με, while the other has a strain sensitivity of + 1.5 pm/με. Shu et al [35] has discussed the sign (positive or negative) of the strain sensitivity of the LPFG by the theoretical analysis and related experiments in more detail.

3.3 bending sensing

The bending response of the HLPFG sample-C has been measured by a setup illustrated in Fig. 6(a), where a metal elastic-beam is employed, both ends of which are braced by two padding-blocks, and keeping the elastic-beam can be bent freely. The optical fiber connected with the sample-C is, mounted on the metal elastic-beam, and kept all movement restriction except along fiber axis-direction freedom. Here, two light weights of 2g are employed to ensure that the grating sample-C stays straight in the whole experiment. The grating sample-C is bent while a displacement, controlled by using a precise micrometer driver, is applied to the middle of metal elastic-beam. The curvature radius of the sample-C can be approximately described by,

$$R^2 = \frac{L^2 + \left(R-d\right)^2}{4} \tag{2}$$

where R is a bent radius of metal elastic-beam under a applied displacement of d by using the precise micrometer driver, and L is the distance between two padding-blocks. So that the corresponding bent curvature can be expressed as,

$$c = \left(\frac{1}{R}\right) = \frac{8d}{L^2 + 4d^2} \tag{3}$$

where L is a pre-set constant of the distance, d is the recorded value of the applied displacement each time. As show in Fig. 6(c), here, the HLPFG sample-C has a resonant wavelength of 1454.2 nm, corresponding to a grating length of 18 mm, grating pitch of 524.5 μm and coupling strength of –35 dB. As shown in Fig. 6(c), the transmission spectral evolution of the sample-C is recorded while the applied displacement of d from 0 mm to 5 mm, i.e. corresponding curvature is from 0 to 9.06 (1/m), respectively. As shown in Fig. 6(b), a bending sensitivity of sample-C is achieved, by a linear fit using the measured data of wavelength changes versus applied curvature, to be 1.94 nm/(1/m), and this result is well below the reported bending sensitivity of LPFG fabricated by CO_2 laser with a slope 12.62 nm/(1/m) [32]. As shown in Fig. 6(c), the coupling strength of the HLPFG sample-C is reduced obviously and background loss is increased slowly with the curvature raising. The reason is that the bending may cause an asymmetric index variation along fiber axis direction owing to photoelastic effect, and the resultant refractive index perturbation increases with the increase of the curvature, the coupling strength and phase matching conditions become sensitive [21,34].

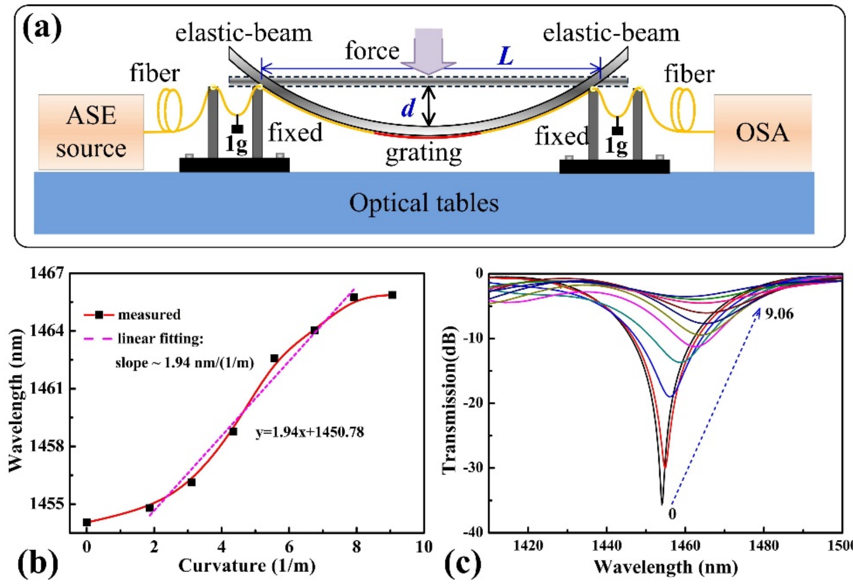

Fig. 6. (a) Schematic diagram of the experimental setup is used for applying bending to the sample-C. (b) The measured resonant wavelength of sample-C as a function of the curvature. (c) The spectral evolution of sample-C with different curvature from 0 to 9.06 (1/m).

4. Conclusion

In conclusion, we demonstrated a high-efficiency grating fabrication system, which is consisted of basic devices, a high-precision rotator, two translational platforms, and a hydrogen-oxygen flame. Such the fabrication system can be used for fabricating a novel helical long period fiber grating (HLPFG) based on residual stress concentration by twisting optical fiber under a fused status. Furthermore, the sensing performances of the HLPFG have been measured, such as, a response of the temperature, bending and tensile strain. The measured results have illustrated that the HLPFG can be developed a high-temperature sensor with a temperature sensitivity of 133 pm/°C. In addition, comparing with the traditional CLPFG created by CO_2 laser, the HLPFG has a lower sensitivity to applied bending and tensile strain, thus, the proposed HLPFG could have a great potential in special applications as optical temperature sensors, which has a lower cross sensitivity induced by bending and tensile strain.

5. Funding

National Natural Science Foundation of China (NSFC) (grant nos. 61425007, 61635007 and 61675137); Guangdong Natural Science Foundation (grant nos. 2015B010105007 and 2014A030308007); China Postdoctoral Science Foundation (grant nos. 2018M63315 and 2016M600669); Science and Technology Innovation Commission of Shenzhen (grant nos. JCYJ20160427104925452, JCYJ20170412105604705 and JCYJ20160307143716576); Research Funding from Shenzhen University (grant no. 2016030), and Development and Reform Commission of Shenzhen Municipality Foundation.

References

1. Y. P. Wang, "Review of long period fiber gratings written by CO_2 laser," J. Appl. Phys. **108**(8), 081101 (2010).
2. A. M. Vengsarkar, J. R. Pedrazzani, J. B. Judkins, P. J. Lemaire, N. S. Bergano, and C. R. Davidson, "Long-period fiber-grating-based gain equalizers," Opt. Lett. **21**(5), 336–338 (1996).

3. A. M. Vengsarkar, P. J. Lemaire, J. B. Judkins, V. Bhatia, T. Erdogan, and J. E. Sipe, "Long-period fiber gratings as band-rejection filters," J. Lightwave Technol. **14**(1), 58–65 (1996).
4. Y. P. Wang, Y. J. Rao, Z. L. Ran, T. Zhu, and X. K. Zeng, "Bend-insensitive long-period fiber grating sensors," Opt. Lasers Eng. **41**(1), 233–239 (2004).
5. R. Y. N. Wong, E. Chehura, S. E. Staines, S. W. James, and R. P. Tatam, "Fabrication of fiber optic long period gratings operating at the phase matching turning point using an ultraviolet laser," Appl. Opt. **53**(21), 4669–4674 (2014).
6. A. Dragomir, D. N. Nikogosyan, K. A. Zagorul'ko, and P. G. Kryukov, "Inscription of long-period fibre gratings by femtosecond UV radiation," in *Optics and Photonics Technologies and Applications*, W.J. Blau, J.F. Donegan, A.F. Duke, J.A. MacCraith, N.D. McMillan, G.M. Oconnor, E. Omongain, V. Toal, J.A. McLaughlin, eds. (2003), pp. 313–320.
7. Y. P. Wang and Y. J. Rao, "CO_2-laser induced LPFG torsion characteristics depending on length of twisted fibre," Electron. Lett. **40**(18), 1101–1103 (2004).
8. Y. P. Wang and Y. J. Rao, "Long period fibre grating torsion sensor measuring twist rate and determining twist direction simultaneously," Electron. Lett. **40**(3), 164–166 (2004).
9. D. D. Davis, T. K. Gaylord, E. N. Glytsis, S. G. Kosinski, S. C. Mettler, and A. M. Vengsarkar, "Long-period fibre grating fabrication with focused CO_2 laser pulses," Electron. Lett. **34**(3), 302–303 (1998).
10. G. Yin, J. Tang, C. Liao, and Y. Wang, "Automatic arc discharge technology for inscribing long period fiber gratings," Appl. Opt. **55**(14), 3873–3878 (2016).
11. Y. Kondo, K. Nouchi, T. Mitsuyu, M. Watanabe, P. G. Kazansky, and K. Hirao, "Fabrication of long-period fiber gratings by focused irradiation of infrared femtosecond laser pulses," Opt. Lett. **24**(10), 646–648 (1999).
12. M. L. von Bibra, A. Roberts, and J. Canning, "Fabrication of long-period fiber gratings by use of focused ion-beam irradiation," Opt. Lett. **26**(11), 765–767 (2001).
13. I. K. Hwang, S. H. Yun, and B. Y. Kim, "Long-period fiber gratings based on periodic microbends," Opt. Lett. **24**(18), 1263–1265 (1999).
14. H. Sakata and K. Yamahata, "Magnetic-force-induced long-period fiber gratings," Opt. Lett. **37**(7), 1250–1252 (2012).
15. M. Yoon, S. Park, and Y. Han, "Simultaneous measurement of strain and temperature by using a micro-tapered fiber grating," J. Lightwave Technol. **30**(8), 1156–1160 (2012).
16. B. H. Kim, Y. Park, T. J. Ahn, D. Y. Kim, B. H. Lee, Y. Chung, U. C. Paek, and W. T. Han, "Residual stress relaxation in the core of optical fiber by CO_2 laser irradiation," Opt. Lett. **26**(21), 1657–1659 (2001).
17. Y. Q. Liu, H. W. Lee, K. S. Chiang, T. Zhu, and Y. J. Rao, "Glass Structure Changes in CO_2-Laser Writing of Long-Period Fiber Gratings in Boron-Doped Single-Mode Fibers," J. Lightwave Technol. **27**(7), 857–863 (2009).
18. A. J. C. Grellier, N. K. Zayer, and C. N. Pannell, "Heat transfer modelling in CO_2 laser processing of optical fibres," Opt. Commun. **152**(4–6), 324–328 (1998).
19. X. P. Wang, D. D. Wang, Q. Wang, L. L. Xian, and L. Li, "Fabrication and characterization of helical long-period fiber gratings in single-mode fibers," Optik (Stuttg.) **158**, 28–32 (2018).
20. R. Subramanian, C. L. Zhu, H. Zhao, and H. P. Li, "Torsion, Strain, and Temperature Sensor Based on Helical Long-Period Fiber Gratings," IEEE Photonics Technol. Lett. **30**(4), 327–330 (2018).
21. X. B. Cao, Y. Q. Liu, K. W. Wang, Q. Q. Wang, and T. Y. Wang, "Fabrication and Sensing Characteristics of Chiral Long-Period Fiber Gratings Written in the Single-Mode Fiber by CO_2 Laser," in *2016 15th International Conference on Optical Communications and Networks* (2017), pp. 1–3.
22. S. Oh, K. R. Lee, U. C. Paek, and Y. Chung, "Fabrication of helical long-period fiber gratings by use of a CO_2 laser," Opt. Lett. **29**(13), 1464–1466 (2004).
23. C. D. Poole, C. D. Townsend, and K. T. Nelson, "Helical-grating 2-mode fiber spatial-mode coupler," J. Lightwave Technol. **9**(5), 598–604 (1991).
24. S. Liu, Y. Zhang, C. Fu, Z. Bai, Z. Li, C. Liao, Y. Wang, J. He, Y. Liu, and Y. Wang, "Temperature insensitivity polarization-controlled orbital angular momentum mode converter based on an LPFG induced in four-mode fiber," Sensors (Basel) **18**(6), E1766 (2018).
25. H. Wu, S. Gao, B. Huang, Y. Feng, X. Huang, W. Liu, and Z. Li, "All-fiber second-order optical vortex generation based on strong modulated long-period grating in a four-mode fiber," Opt. Lett. **42**(24), 5210–5213 (2017).
26. C. L. Fu, S. Liu, Z. Y. Bai, J. He, C. R. Liao, Y. Wang, Z. L. Li, Y. Zhang, K. M. Yang, B. Yu, and Y. P. Wang, "Orbital Angular Momentum Mode Converter Based on Helical Long Period Fiber Grating Inscribed by Hydrogen-Oxygen Flame," J. Lightwave Technol. **36**(9), 1683 (2018).
27. S. Liu, Y. Wang, C. Liao, Y. Wang, J. He, C. Fu, K. Yang, Z. Bai, and F. Zhang, "Nano silica diaphragm in-fiber cavity for gas pressure measurement," Sci. Rep. **7**(1), 787 (2017).
28. V. Bhatia and A. M. Vengsarkar, "Optical fiber long-period grating sensors," Opt. Lett. **21**(9), 692–694 (1996).
29. X. Zhong, Y. Wang, J. Qu, C. Liao, S. Liu, J. Tang, Q. Wang, J. Zhao, K. Yang, and Z. Li, "High-sensitivity strain sensor based on inflated long period fiber grating," Opt. Lett. **39**(18), 5463–5466 (2014).
30. P. Wang and H. Li, "Helical long-period grating formed in a thinned fiber and its application to a refractometric sensor," Appl. Opt. **55**(6), 1430–1434 (2016).

Optics EXPRESS

31. Y. J. Rao, D. W. Duan, Y. E. Fan, T. Ke, and M. Xu, "High-Temperature Annealing Behaviors of CO2 Laser Pulse-Induced Long-Period Fiber Grating in a Photonic Crystal Fiber," J. Lightwave Technol. **28**(10), 1530–1535 (2010).
32. L. Zhang, Y. Q. Liu, X. B. Cao, and T. Y. Wang, "High sensitivity chiral long-period grating sensors written in the twisted fiber," IEEE Sens. J. **16**(11), 4253–4257 (2016).
33. S. Liu, K. Yang, Y. Wang, J. Qu, C. Liao, J. He, Z. Li, G. Yin, B. Sun, J. Zhou, G. Wang, J. Tang, and J. Zhao, "High-sensitivity strain sensor based on in-fiber rectangular air bubble," Sci. Rep. **5**(1), 7624 (2015).
34. Y. J. Rao, Y. P. Wang, Z. L. Ran, and T. Zhu, "Novel fiber-optic sensors based on long-period fiber gratings written by high-frequency CO2 laser pulses," J. Lightwave Technol. **21**(5), 1320–1327 (2003).
35. X. W. Shu, L. Zhang, and I. Bennion, "Sensitivity characteristics of long-period fiber gratings," J. Lightwave Technol. **20**(2), 255–266 (2002).